RECONFIGURABLE INTELLIGENT SURFACE FOR 5G COMMUNICATIONS

A PROJECT REPORT

Submitted by

CB.EN.U4ECE19136 NIGIL M.R

Under the Guidance of

Mr. SABARISH NARAYANAN B

in partial fulfillment of the requirements for the award of the degree of

BACHELOR OF TECHNOLOGY

IN

ELECTRONICS AND COMMUNICATION ENGINEERING

AMRITA SCHOOL OF ENGINEERING

AMRITA VISHWA VIDYAPEETHAM

COIMBATORE 641112

August 2023

AMRITA SCHOOL OF ENGINEERING

AMRITA VISHWA VIDYAPEETHAM

COIMBATORE 641112

BONAFIDE CERTIFICATE

This is to certify that project report entitled "**RECONFIGURABLE INTELLIGENT SURFACE FOR 5G COMMUNICATION**".

submitted by

CB.EN.U4ECE19136 NIGIL M.R

in partial fulfillment of the requirements for the award of the **Degree of Bachelor of Technology** in **ELECTRONICS AND COMMUNICATION ENGINEERING**, is a bonafide record of the work carried out under our guidance and supervision at the Amrita School of Engineering, Coimbatore.

Internal Project Advisor
Mr. Sabarish Narayanan B
Assistant Professor

Project Coordinator
Mr. Pargunarajan K
Assistant Professor

Chairman
Dept. of Elec. & Comm. Engineering

The project was evaluated by us on:

Internal Examiner

External Examiner

DEDICATION

I would love to dedicate this project to my beloved parents and teachers and thanks them for their encouragement and support.

ACKNOWLEDGEMENT

I would like to extend my gratitude to Dr. Madhu Mohan N, Chairperson of the Electronics and Communication department, and Dr. Sasangan Ramanathan, Dean, School of Engineering, Amrita Vishwa Vidyapeetham for allowing me to do the industrial project as a part of my final year project.

I would like to thank my internal project guide Mr. Sabarish Narayanan B for the support and guidance he has provided throughout the project. I would also like to thank my class advisor Mr. Pargunarajan K.

Last but not the least, I would like to thank my parents and my friend Mr. Sudeep Bhattacharya (PhD, IIT Kanpur) and my classmate Rahul Raja R.

I acknowledge that this project was completed solely by me and not by other individual or group.

ABSTRACT

The growth in technology requires a lot of new inventions along with improvements in existing devices and systems. Constant growth in wireless communication around the world demands a wider spectrum of operation. With growing frequency ranges, the possibility of fabricating devices for higher frequencies is hindered by many factors and as far as the cellular communication is concerned, setting up cell sites have become increasing costlier and requires high maintenance. With increase in the number of wireless devices it is not possible to deploy cell sites at multiple location and shadow regions. On of the alternate this is the reconfigurable intelligent surface, these surfaces when deployed serves the function of an sector antenna and also produces beam steering capabilities and high directivity when active components are incorporated. For designing RIS surfaces metamaterials are considered to be the ideal candidate.

In this project, a passive 4x4 RIS is design and simulated at Sub-6 GHz by using an optimized metamaterial split resonator structure with tunability of surface achieved using varactor diodes.

TABLE OF CONTENTS

LIST OF SYMBOLS

SYMBOL	DESCRIPTION	PAGE NO
ε_{effz}	Effective Permittivity	10
ω_p	Plasma Frequency	10
Γ	Reflection Coefficient	10
p	Lattice Constant	10
λ	Wavelength	10
μ_{effz}	Effective Permeability	11
γ	Loss Factor	11
ω_0	Resonant Frequency	11
n_{effz}	Effective Refractive Index	13
ω_{mp}	Magnetic Plasma Frequency	13
ω_{ep}	Electric Plasma Frequency	13
ω_{eo}	Electric Resonant Frequency	13
ω_{mo}	Magnetic Resonant Frequency	13
ε_r	Relative Permittivity	23
L_{SUB}	Substrate Length	23
h	Substrate Thickness	23
c	Speed of Light	23
f_{SRR}	Operation Frequency of Split Resonators	23-24
d	Gap Width	19-25

LIST OF ABBREVIATIONS

ABBREVIATION	EXPANSION	PAGE NO
ARIS	Active Reconfigurable Intelligent Surface	3
CRLH	Composite Right- and Left-Hand Material	14
DAC	Digital to Analog Converter	3
ENG	Epsilon Negative Material	9
FE-BI	Finite Element Boundary Integral	2
FSS	Frequency Selective Surface	2
IoT	Internet of Things	3
LHM	Left Hand Material	14
MNG	Mu Negative Material	10
NIM	Negative Refractive Index Material	12
PRIS	Passive Reconfigurable Intelligent Surface	3
RHM	Right Hand Material	14
RIS	Reconfigurable Intelligent Surface	2
SDM	Software Defined Metasurfaces	2
SR	Split Resonators	2
TL	Transmission Line	16
UE	User Equipment	3
WR90	Waveguide 90	2

LIST OF FIGURES

LIST OF TABLES

CHAPTER 1

INTRODUCTION

1.1. PROJECT OBJECTIVE

The proposed work is aimed at creating a Reconfigurable Intelligent Surface (RIS) for 5G Communication, Intelligent Reflective Surface (IRS) or Software Defined Metasurfaces (SDM). These are a type of reflect array surface used mainly in higher-generation wireless communication beyond 4G LTE for beam steering. The RIS can be made of various materials, which include metals, ferroelectric materials, liquid crystals, graphene, carbon-based materials, phase change materials, frequency selective surfaces (FSS), tuneable metamaterials, non-linear metamaterials, chiral metamaterials, and metasurfaces. This work focuses on using engineered electromagnetic materials called metamaterials with tunability to realize RIS. Metamaterials are artificially engineered materials capable of exhibiting electromagnetic properties that are not found in nature. There are various kinds and shapes of metamaterials available; this work is realized using a conventional and most commonly used metamaterial called split resonators (SR).

Metamaterial tunability is usually achieved by incorporating PIN diodes or varactor diodes. These diodes are mounted to the designed substrate such that they are capable of altering the physical properties of the dielectric substrate. This work employs the varactor diode to achieve tuneable metamaterials. By appropriately controlling the capacitance of the varactor diode using the bias voltage, the medium index of the dielectric substrate can be altered. This altered dielectric medium provides both magnitude and phase change to the reflective electromagnetic wave. The first part of the work contains simulation and design of a simple metamaterial model for the sub-6 GHz range using Ansys Electronic Desktop (AEDT) in Floquet mode. Following the simple metamaterial simulation, an equivalent circuit of a varactor diode is mounted on the model and tested for changes in magnitude and phase by changing the capacitance using the Ansys AEDT-optimized parametric sweep. Similarly, various types of existing SR geometries are simulated and tested for better tunability using Keysight Advance Design System (ADS).

Expanding on the work, an 8x8 array is created with the most tuneable SR, and by using the Finite Element Boundary Integral Method (FE-BI), a hybrid simulation technique that uses the horn antenna Waveguide Rectangular-90 (WR90), which is similar to a conical sector antenna used in wireless communication, is used to mimic

the real-time scenario and test for phase angle change in the reflected beam. As a final part of the proposed work, a Verilog code is created to control the biasing voltage of the varactor diode based on the beam angle requirement. But, along with this function to realize a function RIS, many other hardware components, including actuators and sensors, are needed to adjust reflective elements, Digital to Analog converters (DACs), control logic for intelligent surfaces, and finally interface all these to create a complete system-level design. This complete fabrication and realization of a working RIS goes beyond the scope of the project.

In the upcoming section, a summary of the current trends in wireless communication systems, the need for reconfigurable surfaces, the advantages that are achieved using RIS surfaces, and the basic workings of a RIS will be presented. In Chapter 2, an overview of metamaterials, their classification, and the various types of metamaterials used for RIS are provided. In Chapter 3, a brief note on various types of split resonators is provided, and in the final Chapter 4 using the best SR structure an 4x4 PRIS is designed and simulated using Ansys AEDT.

1.2. WIRELESS COMMUNICATION BEYOND 4G LTE

In today's world the internet of things (IoT) has hooked up beyond 30 billion devices connected to the internet. The number of devices is expected to reach 100 billion users by 2030. With such exponentially growing trend, the wireless communication systems have the potential to scale and support this trend. With the advent of 5G communication, the spectrum 1 GHz to 5 GHz has been utilized and currently the trend is moving towards the sub-6 GHz region. For users to have high speed connectivity in the sub-6 GHz and beyond, cell sites cannot be deployed everywhere, this when efficient solution like reconfigurable intelligent surface comes into play, with their capability to control the propagation of radio waves providing reliable data transfer in the remote and dark zones. With the increasing demand for higher data rates, lower latency and increased network capacity, RIS offers promising solution providing the following advantages over tradition wireless communication systems [1].

1. Spectrum Efficiency and Capacity Enhancement
2. Beamforming and Massive MIMO

3. Coverage Extension and Filling Dead Zones
4. Energy Efficiency
5. Adaptive and Reconfigurable Networks
6. Enhanced Security and Privacy
7. Cost-Effectiveness
8. Enables 6G Communication

There are usually two types of RIS structures: passive RIS (PRIS) and active RIS (ARIS). The passive RIS surface will not embed any active components like the amplifiers; they use passive components such as tuneable capacitors, tuneable inductors, etc. to provide the phase shift required, whereas in the Active RIS (ARIS), the incident radio waves are amplified and steered to the desired user equipment. This is shown in Figure 1.1 [1, 2].

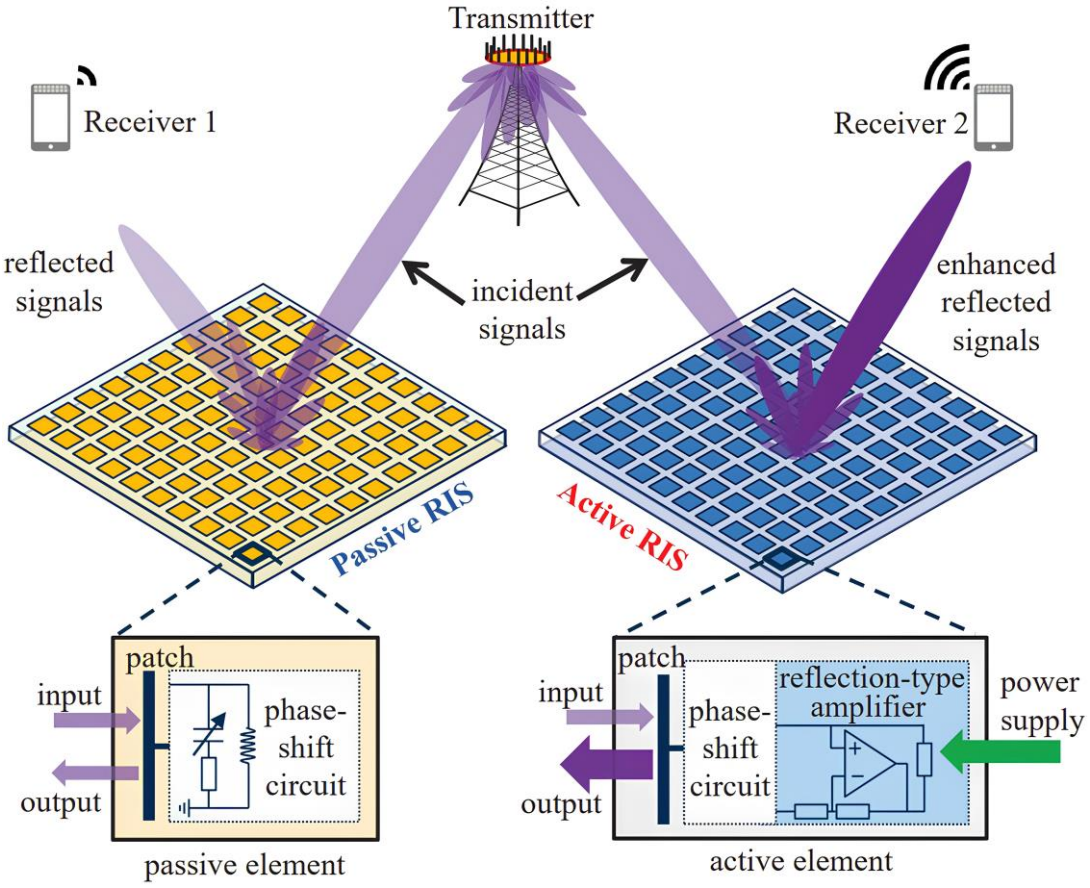

Fig 1.1 Passive and Active Reconfigurable Intelligent Surface (RIS)

The visual interpretation of the basic functionality of a RIS is provided in Figure 1. The transmitted radio waves are incident on the RIS, and based on the presence of the user equipment (UE) or crowd cluster, the sensors embedded in the RIS provide

input to the FPGA. With the necessary information, the passive or active circuit is excited with the appropriate voltage, and the reflected beam angle is steered in the direction of the UE due to a change in the properties of the surface, usually the refractive index of the surface [2]. This is a basic description of the workings of a RIS surface. As mentioned in the previous section, the physical realization of the RIS is a huge task that involves system-level design that contains all the signal processing, logic controls, and sensing elements. The tuneability described here is usually achieved by a special class of electromagnetic materials called metamaterials. A detailed summary of the design and properties of these metamaterials is provided in the next section.

CHAPTER 2

METAMATERIALS AND DESIGN APPROACHES

2.1. METAMATERAILS

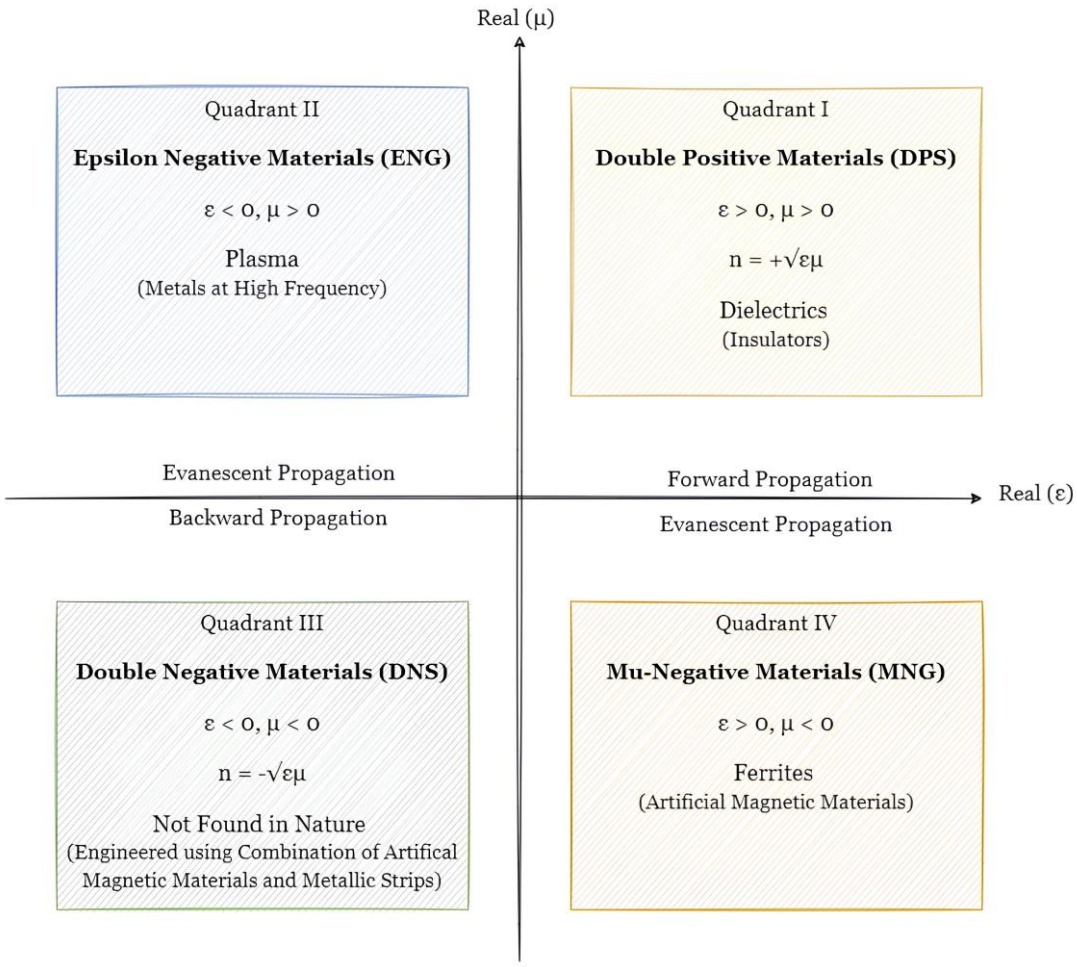

Fig 2.1 Classification of Metamaterials

Metamaterials are man-made materials comprising subwavelength resonating structures that can manipulate light waves. Unlike conventional materials, which rely on atoms or molecules, electromagnetic metamaterials are predominantly derived from these subwavelength resonating structures. The term “metamaterial” was coined by Walser to describe artificial three-dimensional periodic composites capable of exhibiting multiple electromagnetic responses not commonly found in nature. Consequently, they are also referred to as engineered materials. Metamaterials can be designed to operate at specific frequencies and exhibit a diverse array of electromagnetic properties, incorporating characteristics absent in naturally occurring materials. This led to the creation of the term “meta,” signifying “beyond materials [3].”

Victor Veselago was the scientist to propose a classification system for metamaterials, based on the permittivity and permeability of homogenous materials.

When both permittivity and permeability are negative, several phenomena such as Snell's law, the Cerenkov effect, and Doppler shift deviate and exhibit reversed behavior [3]. Figure 1.2 shows the metamaterials classification on the basis of their permittivity and permeability values.

Quadrant 1 - Dielectrics are commonly found in a domain where both the real electric permittivity and magnetic permeability are positive.

Quadrant II - Interactions between radiation and plasma generally occur in regions well beyond the infrared range and result in negative permittivity. For instance, metamaterial like thin-wire arranged in periodically, where the periodicity is less than the wavelength then they can act as dilute plasma, leading to negative permittivity effect.

Quadrant III - Negative permeability values are rare in nature and can be achieved through magnetic resonances in ferromagnets. The most famous negative permeability structure is the split-ring resonators (SRRs) and cut wire pairs exhibit negative permeability when interacting with magnetic waves.

Quadrant IV - By precisely tuning the electric and magnetic responses, it becomes possible to create double negative materials with negative permittivity and permeability at the same frequency. However, such materials are seldom observed in nature due to their very narrow and distinct frequency range for the realization of negative permeability and negative permittivity.

The following Sections 2.1 provides an overview of the various types of metamaterials and properties of the metamaterials.

2.1.1. EPSILON NEGATIVE (ENG) MATERIALS

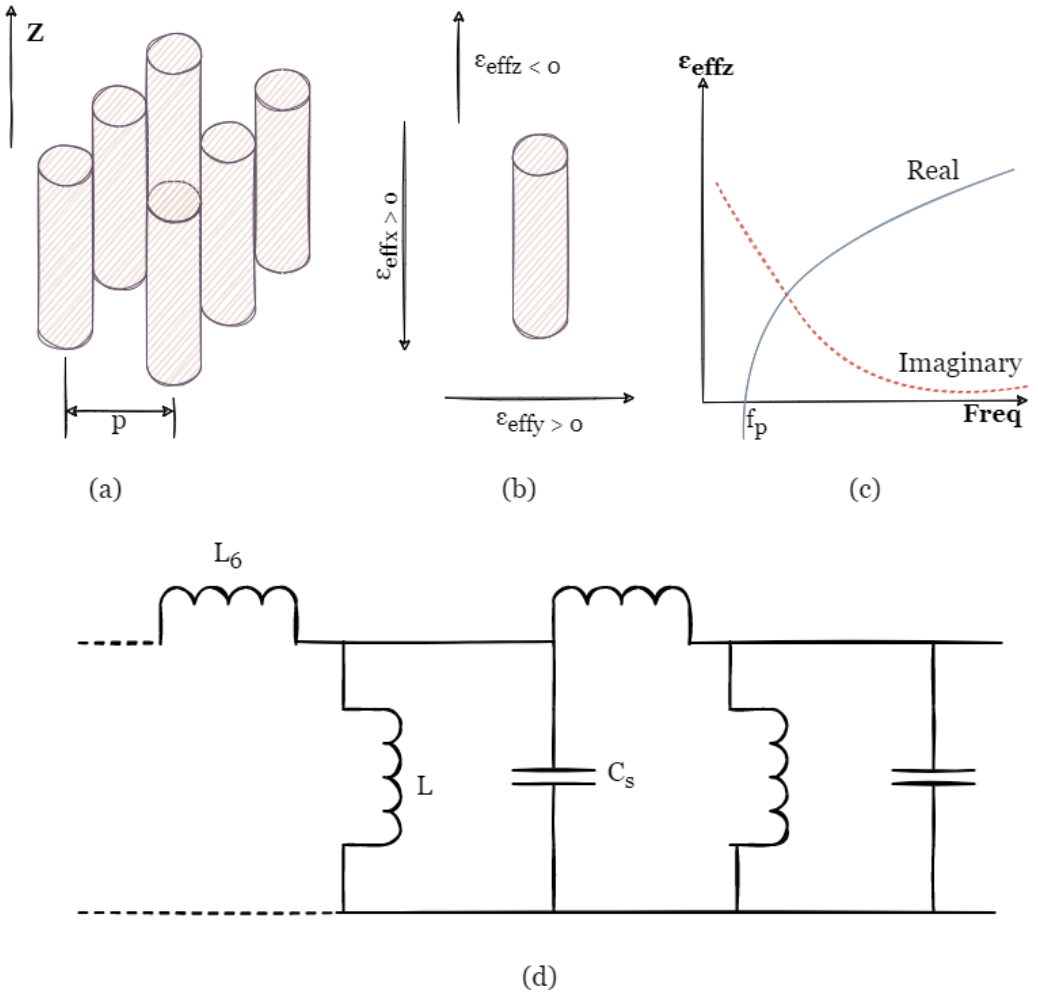

Fig 2.2 (a) Conducting Metallic Wire Array, (b) Unit Cell, (c) ε_{effz} Plot and (d) Equivalent TL Circuit Model

Epsilon-Negative Metamaterials (ENG) are materials characterized by a negative value of ε and a positive value of μ. The negative permittivity value in ENG metamaterials is accomplished through the use of a metallic mesh composed of thin wires. This metallic mesh acts as a high pass filter (HPF) for incident plane waves with electric fields parallel to the thin wires [3]. The cylindrical array formed by these wires exhibits negative permeability below the plasma frequency. The metallic wire mesh can be constructed using metals like copper, aluminum, silver, or gold. These metallic structures are arranged in periodic patterns where the periodicity is less than the intended wavelength, this is depicted in Figure 2.2a. The individual unit cell structure

of the thin wire is illustrated in Figure 2.2b. Figures 2.2c and Figure 2.2d showcase the effective permittivity ε_{effz} graph and LC equivalent circuit of the thin wire metamaterial, respectively.

$$\varepsilon_{effz} = 1 - \frac{{\omega_p}^2}{\omega\,(\omega + j\Gamma)} \tag{2.1}$$

Where, ω_p is the plasma frequency, ω is the propagation frequency of the EM wave and Γ is the reflection coefficient.

The permittivity becomes negative when the propagation frequency is below the plasma frequency, as described in Equation 2.1 above. As the propagation frequency approaches the plasma frequency, the effective permittivity value increases. At the plasma frequency, the effective permittivity becomes precisely zero, resulting in a refractive index of zero.

Below the cut-off frequency, there is no wave propagation and the electromagnetic waves are entirely reflected back. The plasma frequency is determined by the lattice constant p and the wire radius. For the wire array to be considered an equivalent continuous plasma, the lattice constant should be smaller than the wavelength as in Equation 2.2.

$$p \ll \lambda \tag{2.2}$$

The above condition allows the wire array to be treated as a continuous electric plasma.

2.1.2. MU-NEGATIVE (MNG) MATERIALS

Mu-Negative Metamaterials (MNG) are materials characterized by a positive value of ε and a negative value of μ. Among various structures used for creating mu-negative (MNG) materials, the split ring resonator (SRR) has emerged as the most preferred choice. The SRR unit cell consists of two concentric metallic rings, typically circular but sometimes of other shapes as well, with a gap d separating them [3]. On each side of the rings, there are tiny slits spaced 180^o apart, as depicted in Figure 2.3a.

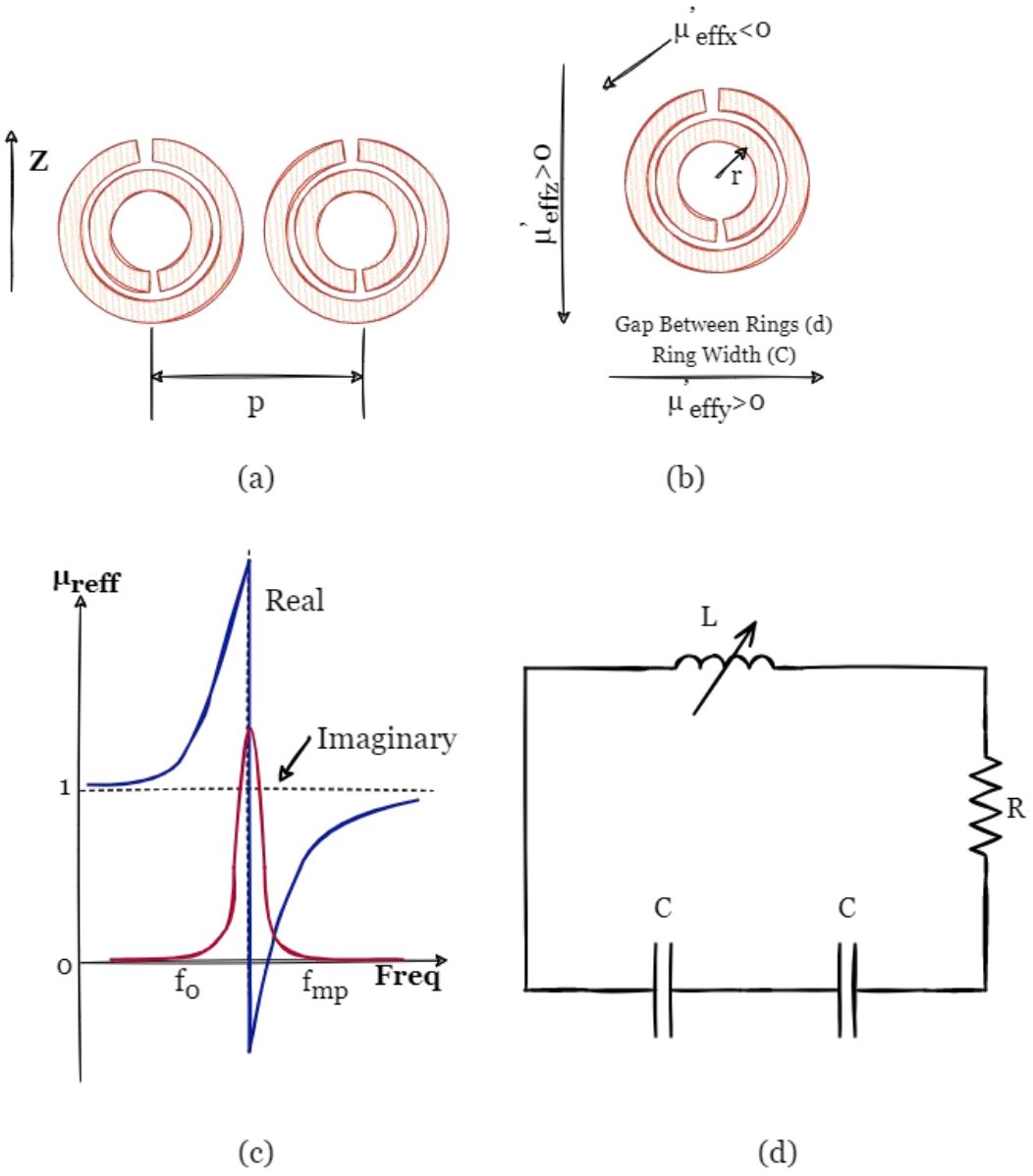

Fig 2.3 (a) SRR Array, (b) SRR Unit Cell, (c) μ_{effz} Plot and (d) Equivalent TL Circuit Model

Figure 2.3b indicates that the gap between the inner and outer rings functions as a capacitor, while the rings themselves act as inductors when current passes through them, accordance with Faraday's law of electromagnetic induction. Consequently, the two rings collaborate to create LC resonance circuits. The effective permeability of a SRR is given by the Equation 2.3.

$$\mu_{effz} = 1 - \frac{{\omega_p}^2 - {\omega_0}^2}{\omega^2 - {\omega_0}^2 - j\gamma\omega} \tag{2.3}$$

Where, ω_p is the plasma frequency, ω_0 is the resonance frequency of the ferrite material, ω is the frequency of the incident wave and γ is the losses.

The frequencies ω_0 and ω_p are determined by the lattice constant ρ and various geometrical variables of the Split Ring Resonator (SRR). These geometrical variables include the inner and outer radius of the rings, the spacing between the rings, and the width of the slits. Figure 2.3c illustrates the effective permeability plot, while Figure 2.3d depicts the equivalent resonance circuit. These plots and circuits provide valuable insights into the behavior and characteristics of the SRR-based metamaterial.

2.1.3. NEGATIVE INDEX MEDIUM (NIM) MATERALS

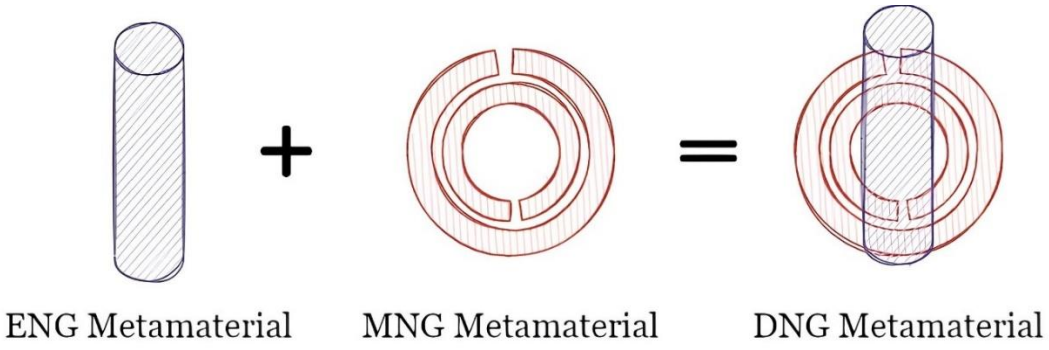

Fig 2.4 Combination of Thin Metallic Strip and Split Ring Resonator forming Double Negative Material

Negative refractive index materials (NIM) or Double Negative (DNG) materials are characterized by having both negative ε and μ values. The achievement of DNG metamaterial capabilities was initially accomplished by combining the thin wire-based ENG structure with the SRR-based MNG structure, as depicted in Figure 2.4. This combination of SRR and wire medium creates an artificial dielectric that fulfills the requirements for both negative ε and μ [3, 4, 5]. Moreover, to exploit the benefits of both sides of the dielectric layer, 2D metamaterials have been developed by etching SRR on one side and a planar strip on the other.

The DNG metamaterial is formed by the synergy of thin wire and SRR components, which exhibit strong resonance behavior, significantly influencing the operating frequency. Consequently, the created DNG metamaterials display a high degree of frequency dependence, leading to the refractive index being expressed as:

$$n = n_{effz}(\omega) = \sqrt{\varepsilon_{effz}(\omega)\mu_{effz}(\omega)} \quad (2.4)$$

Equation 2.4 reveals the relationship between effective permittivity and permeability, establishing the effective refractive index n_{effz} as a function of frequency (ω). The effective permeability and permeability plots are shown in Figure 2.5a and 2.5b, the plot provides the graphical representation of Equation 2.1 and Equation 2.2. These plots provide valuable insights into the frequency-dependent behavior of the metamaterial and its electromagnetic properties.

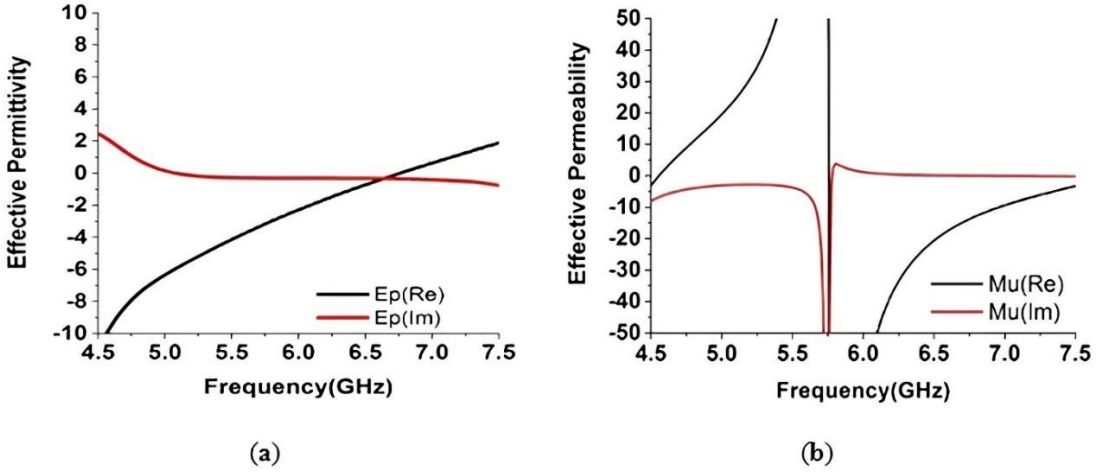

Fig 2.5 Effective Permittivity Plot (a) and Effective Permeability Plot (b) of Negative Index Material

To create Double Negative (DNG) materials, the negative sections of both the ENG structure $(\omega_{eo} < \omega < \omega_{ep})$ and MNG structure $(\omega_{mo} < \omega < \omega_{mp})$ must coincide. Where the later denotes the electric resonant frequency and electric plasma frequency and the former parameters denote the magnetic resonant frequency and plasma frequency [3, 4, 5].

In recent years, these double-negative materials, also known as left-handed materials (LHMs), have garnered significant attention among researchers. They can be modeled as transmission line (TL) structures and resonators, making them easily realizable in physical applications. In practical scenarios, these materials exhibit left-handed material characteristics in certain frequency ranges while displaying right-handed material properties (similar to natural electromagnetic materials) in others.

Caloz et al. coined the term CRLH metamaterials to describe these features. A transmission line modelling approach is used to analyze CRLH metamaterials. The equivalent TL models of one, two, and three-dimensional CRLH metamaterials are developed by utilizing simple inductors and capacitors. A right-handed transmission line model is illustrated by a low pass arrangement of series inductors and parallel capacitors, whereas a left-handed transmission line model is illustrated by a high-pass arrangement of series capacitors and parallel inductors, resulting in group velocity and phase velocity opposing each other, resulting in a left-handed transmission line model.

To provide the readers with more intuitive and comprehensive information about the benefits of metamaterials, the second half of the chapter is focused on summarizing the improvements achieved in antenna performance by the inclusion of metamaterials. In the next section, various design and fabrication approaches for metamaterials are summarized.

2.2. DESIGN APPROACHES

The performance of metamaterials can be influenced by several factors, with metals and dielectrics playing a significant role in energy dissipation. For optimal electromagnetic responses across a wide frequency range, it is essential for metals to be good conductors and dielectric materials to be good insulators. To meet specific requirements such as minimal losses, industrial manufacturing needs, and 3D operation, suitable fabrication procedures must be chosen for each frequency band. For designing a metamaterial usually there are three approaches, the following are:

1. Resonant Approach
2. Transmission Line Approach
3. Hybrid Approach

2.2.1. RESONANT APPROACH

The resonant approach is commonly used for designing highly dispersive resonant structures with narrow bandwidths and losses. It involves merging two distinct particles into a unit cell, the first one with negative permittivity (ENG metamaterial)

and the other one with negative permeability (MNG metamaterial). SRR-based structures are often utilized due to the resonant behavior of the unit cell. In this method, an array of SRRs can exhibit filtering properties and inhibit signal propagation when properly polarized, providing an effective way to reject a frequency band near its quasi-static resonance. A microstrip line loaded with SRRs can create a single-negative medium with stop-band characteristics, suitable for filters and frequency selective surfaces, albeit with limitations on frequency ranges.

This is the approach employed to design the SRR in the upcoming section. The resonant approach uses deign formulas based on the resonant frequency to arrive at optimized dimension for the standard metamaterial structures like the split ring resonator. With the obtained dimension a simulation model is created and fine-tuned to achieve the desired frequency of operation. In this project the design is considered to be resonating in the X-band especially at 10 GHz.

2.2.2. TRANSMISSION LINE APPROACH

The transmission line approach is used to design non-resonant structures with low loss, broad bandwidth, and moderate dispersion. It involves using the transmission line theory to study and create traditional (RH) materials. In this method, the concept of dual transmission line equivalent circuits is applied to analyze and develop LH metamaterials. When the unit cells are much smaller than the propagating signal wavelength, the structure can be considered homogeneous, and the effective permittivity and permeability can be estimated. A dual transmission line with negative effective permittivity and permeability operates as an LH transmission line within a specified frequency band. Since pure LH configurations are not possible due to inherent RH parasitic elements, a composite right/left-handed (CRLH) arrangement is used to depict structures with LH properties. This approach has been used to create various devices, including couplers, planar lenses, and leaky wave antennas, but it may result in substantial insertion losses. To address this, super-compact LH unit cells, like the S-spiral LH unit cells, with minimal insertion loss and high-quality factor at the resonant frequency, are employed.

Note that there is also another approach called the hybrid approach which combines the best of both the resonant model and transmission model but, it is not

detailed here because it is beyond the scope of the project. As mentioned above the design of SRR is carried out using the resonant approach but, the transmission model is used to understand the capacitive and inductive effect due to the gaps and geometrical structures.

CHAPTER 3

TUNABLE UNIT CELL DESIGN AND SIMULATION

3.1. SPLIT RESONATORS - DESIGN APPROACH

In the above sections, the basics of metamaterials and common design approaches were briefed. In this section, by using the resonant based approach various geometrical shapes are considered. Circular, square, triangle, pentagon, hexagon, octagon, omega and decagon are the shapes considered. According to Filippo Costa et al. the tunability of a material can be measured by independently controlling the voltages of unit cell, the phase and amplitude profiles can be accurately synthesized in order to shaping and controlling the reflected fields. The suitable structure for passive RIS design is decided by the distance between two S11 (dB) plots. In terms of design various assumption, simplification is done and in consideration of fabrication various design parameters are fixed.

After the basic design, the design non-fixed design parameters are adjusted such that the resonance occurs at the X-band between the range 9 GHz to 11 GHz after the incorporation of the varactor diode in the gaps of split resonators.

3.2. DESIGN SIMPLIFICATION

3.2.1. RINGS

The primary design simplification is the use of single split ring resonator rather than using double or multiple split ring resonators. By increasing the split rings, the effective capacitance is increased because the additional ring is modelled as series capacitance. Also, the rings provide multi-band resonance making the modelling of optimized PRIS difficult. Hence in order to avoid complications in design, single split ring is considered [6, 7]. But, the double or multi ring resonators can be pursued in the future researchers. A comprehensive comparison between single ring split resonator and double ring split resonator is given in Table 3.1. Note that the concept of double ring split resonator can be extended to multi-ring resonators.

Table 3.1 Comparison Between Single Ring and Double Ring Configurations

Aspects	Single Ring Split Resonator	Double Ring Split Resonator
Resonance	Exhibits only one resonant frequency due to the single split.	Exhibits two distinct resonant frequencies due to the two splits.
Modes	Only one mode of resonance is present.	Dual mode of resonance provides multiple frequency bands.
Tuning Range	Limited tuning range due to the single mode of resonance.	Offers a wider tuning range due to dual mode of resonance.
Coupling and Interaction	Less interaction between the single split ends.	Interaction and potential coupling between the two splits.

Note that increasing the number of splits in a single ring and also incorporating resonating circuit elements can also lead to multi-band resonance.

3.2.2. TUNABLE DIODES

Various literatures have reported using both PIN diodes and Varactor diodes for achieving tunability. Considering the flexibility achieved by incorporating varactor diode, tunabililty range and frequency of operation, the design is done using varactor diodes. A brief comparison between the PIN diode and Varactor diode in terms application in tunability is provided in Table 3.2.

Table 3.2 Comparison Between PIN Diode and Varactor Diode

Aspects	PIN Diode	Varactor Diode
Tunability	Limited tunability is offered.	High tunability because can operate over long range of voltage.
Voltage Requirements	Requires large amount of bias voltage for switching states.	Requires a low bias voltage for tuning and also provides smaller tuning ranges.
Tuning Frequency	Typically used for tuning in MHz to low GHz range.	Frequency tuning range can vary from few MHz to tens of GHz.
Switching Speed	PIN diodes offer faster tunability and switching.	Typically, slower tuning and switching due to voltage dependent capacitance.
Control Signal	For PIN diodes the control signal is current.	Varactor diodes are controlled by voltages.

From the Table 3.2 in can be easily concluded that using the varactor diode offers better tunability and tuning range [8]. In the next section, the technique used to incorporate the varactor diode in the design is briefed along with the circuit model.

3.2.3. VARACTOR DIODE MODEL

In terms of realizing varactor diode in the Ansys AEDT two methodologies were considered, the circuit-based approach called the co-simulation model and the lumped RLC boundary-based approach [8] . Both, the approaches were implemented using the equivalent circuit model of a varactor diode, which is a typical RLC circuit as shown in Figure 3.1.

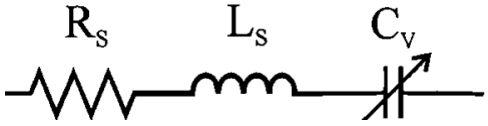

Fig 3.1 Equivalent RLC Model of Ideal Varactor Diode

The varactor diode considered in the design was Infineon Technologies BB6X9 Series. The varactor diodes usually offer tunability from 1 pF to 33 pF for a voltage range of 1 Volt to 50 Volts. In the design, the series inductance L_s in considered as 10 nH, the series resistance is 0.65 Ohms and instead of using the non-linear relationship for the tunable capacitance for reducing complexity of design a linear relation model is created between the voltage and capacitance. The junction capacitance usually in parallel connection with the series resistance is assumed to be zero. The series inductance was short circuited after performing simulation, which provided spurious effect to the existing resonance curve.

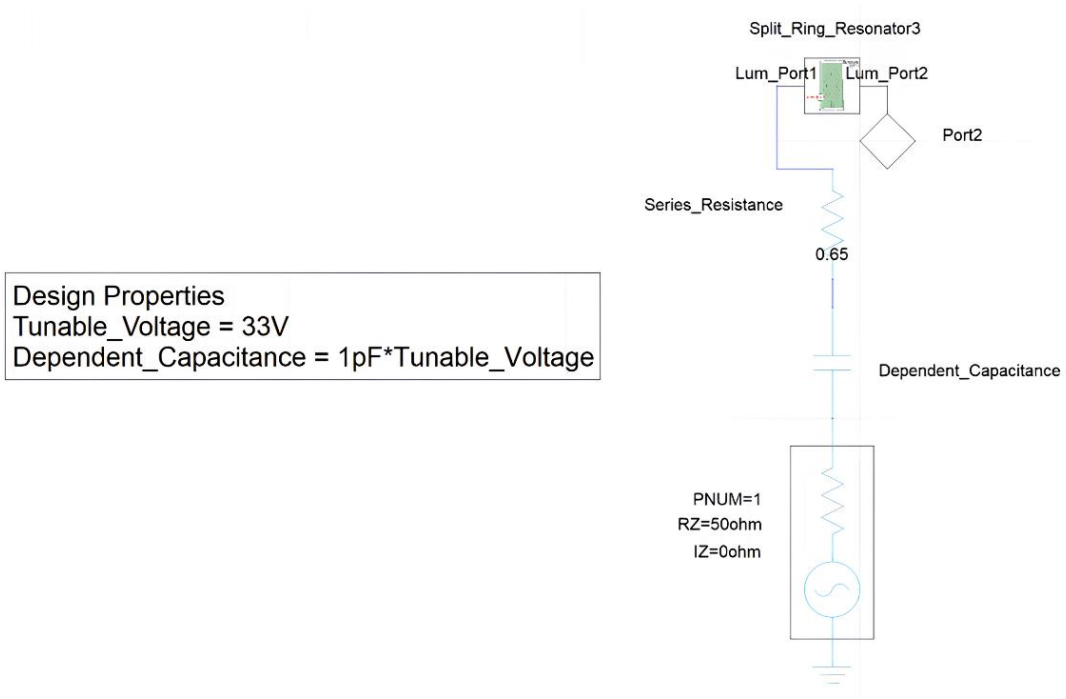

Fig 3.2 Varactor Diode RLC Model Implemented using Ansys AEDT Co-Simulation Model

Though the circuit model proves to be an effective way of modelling in terms of simulation using the lumped RLC model offers flexibility in sweeping the capacitance value and plotting the scattering matrix. Figure 3.2 and Figure 3.3 shows the two types of design considerations employed for incorporating tunability to the design split resonators [8, 9].

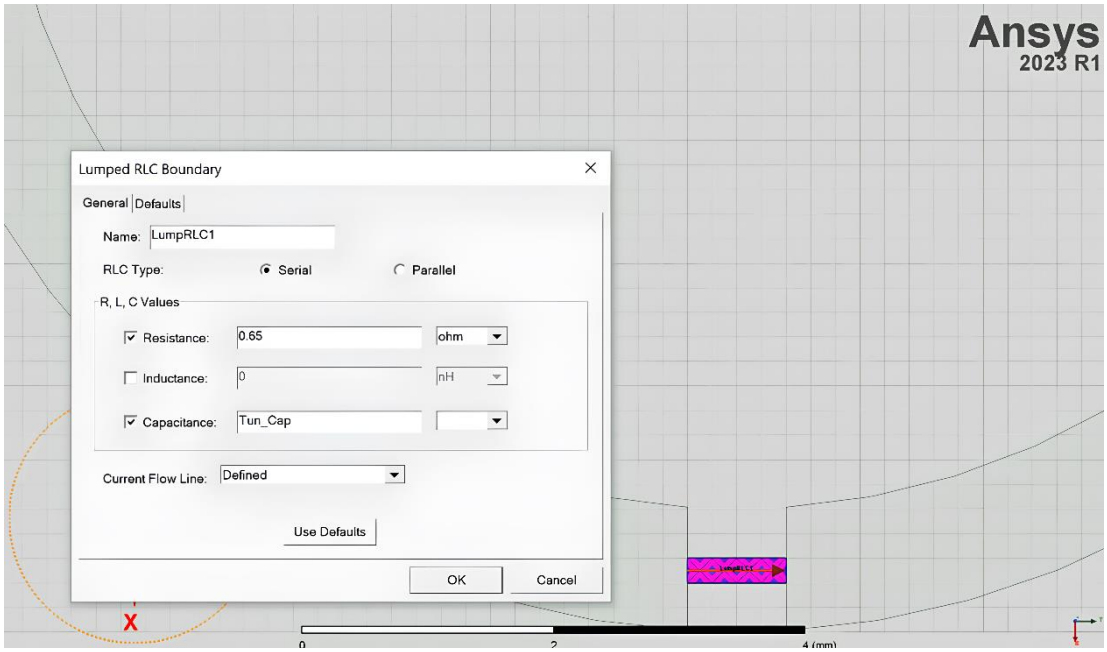

Fig 3.3 Varactor Diode RLC Model Implemented Ansys AEDT Lumped RLC Boundary Approach

In the next section, the basic unit cell is of various shapes are designed, simulated with standard design parameters and compared for optimal performances.

3.3. DESIGN PARAMETERS

3.3.1. STANDARD SUBSTRATES

In the design, substrate material, substrate thickness was fixed based on the market material availability standard. The substrate material is considered as FR4 Epoxy which as a relative permittivity of 4.4 and the substrate thickness is fixed at 1.5 mm.

3.3.2. FIXED MODELLING PARAMETERS

For comparing various design for their tunability performance various design parameters were fixed in the previous section the substrate thickness and substrate material was fixed based on market standards. Based on the operational frequency range in the X-band which is considered as Sub-6 GHz ranges in wireless communication industry, the substrate length is assumed to be 15 mm x 15 mm and the gap (d) of the

split resonators are fixed at 1 mm. Table 3.3 shows all the design parameters that were modelled based on the market standard and for efficient comparison.

Table 3.3 Design Parameters

Modelling Parameter	Parameter Value
Dielectric Constant	FR4 Epoxy (4.4)
Substrate Thickness	1.5 mm
Gap Length	1 mm
Substrate Cross Section	16 mm x 16 mm

3.4 CIRCULAR & SQUARE SPLIT RESONATORS – DESIGN

In the design of split ring resonators, the circular and square resonators serve as the basic for all the other split resonator design patches uses. In section 3.4.1 and 3.4.2 the formula used for designing a square and circular split resonators are given.

3.4.1. SQUARE SPLIT RESONATORS

$$\varepsilon_{effz} = \frac{\varepsilon_r + 1}{2} + \frac{\varepsilon_r + 1}{2}\sqrt{1 + \frac{12h}{L_{SUB}}} \tag{3.1}$$

Where ε_{eff} is the effective permittivity, ε_r is the relative permittivity, h is the thickness of the substrate and L_{SUB} is the dimension of the substrate.

$$L_{OUTER} = \frac{c}{2f_{SSRR}\sqrt{\varepsilon_{eff}}} \tag{3.2}$$

$$L_{INNER} = L_{OUTER} - d \tag{3.3}$$

L_{OUTER} is the side length of the square and L_{INNER} is the side length of the inner square, obtained by subtracting with the gap thickness d. Here f_{SSRR} is the operation frequency.

Using the Equation 3.1 the ε_{eff} is found to be 37. Using Equation 3.2 and Equation 3.3 the side length L of the square is calculated for operation at 10 GHz. The calculated values are given in Table 3.4.

Table 3.4 Calculated Design Values for SSRR

	Calculated Value	**Design Value (Optimized)**
Side Length	16.5 mm	15 mm
Inner Square	15.5 mm	14 mm

3.4.2. CIRCULAR SPLIT RESONATORS

$$R_{INNER} = \frac{c}{2f_{CSRR}\sqrt{\varepsilon_{eff}}} \tag{3.4}$$

$$R_{OUTER} = R_{INNER} + d \tag{3.5}$$

R_{OUTER} is the radius of the outer circle and R_{INNER} is the radius of the inner circle. The R_{OUTER} is obtained by adding the inner radius with the gap thickness d. Here f_{CSRR} is the operation frequency [7].

Using Equation 3.4 and Equation 3.5 the radius of the outer circle and inner circle are calculated for operation at 10 GHz. The calculated values are given in Table 3.5.

Table 3.5 Calculated Design Values for CSRR

	Calculated Value	**Design Value (Optimized)**
Outer Circle Radius	5.98 mm	6 mm
Inner Circle Radius	4.98 mm	5 mm

3.4.3. OTHER DESIGNS

Equilateral Triangle - In case of the triangle split resonator, the side length is considered to be the same length as the square and for the altitude of the triangle is calculated using the below Equation 3.6.

$$Altitude = \frac{L\sqrt{3}}{2} \tag{3.6}$$

Other designs like the pentagon, hexagon, octagon, omega and the decagon the radius of the circumscribed circle is considered to be in same radius as calculated for the circular ring resonator. With some tweaking in the dimension the structures were made to resonate at the desired X-band range.

3.5. UNIT CELL - SIMULATION

For the simulation of metamaterial unit cell, a special port technique called the Floquet Port is used. These ports are mainly used in two cases, firstly they are used to provide excitation to passive surfaces like the frequency selective surface (FSS) and reconfigurable intelligent surface (RIS) etc. and secondly, they are employed in CEM to simulate the behavior of structures that exhibit periodicity or periodic boundary conditions.

3.5.1. CIRCULAR SPLIT RING RESONATOR

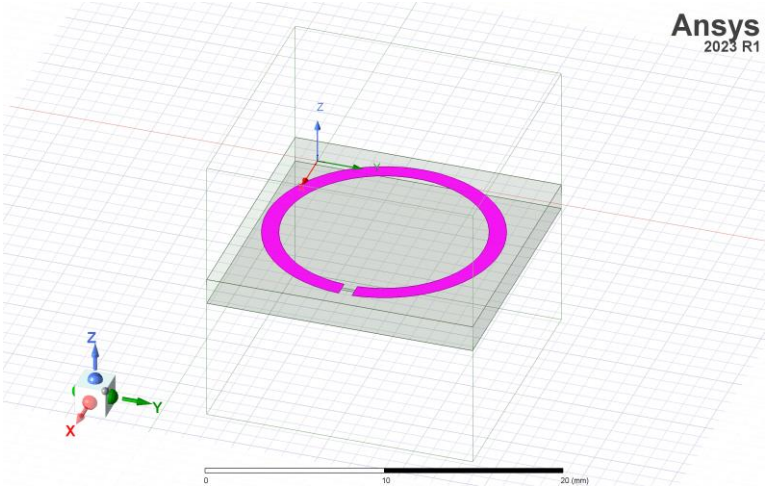

Fig 3.4 Circular Split Ring Resonator

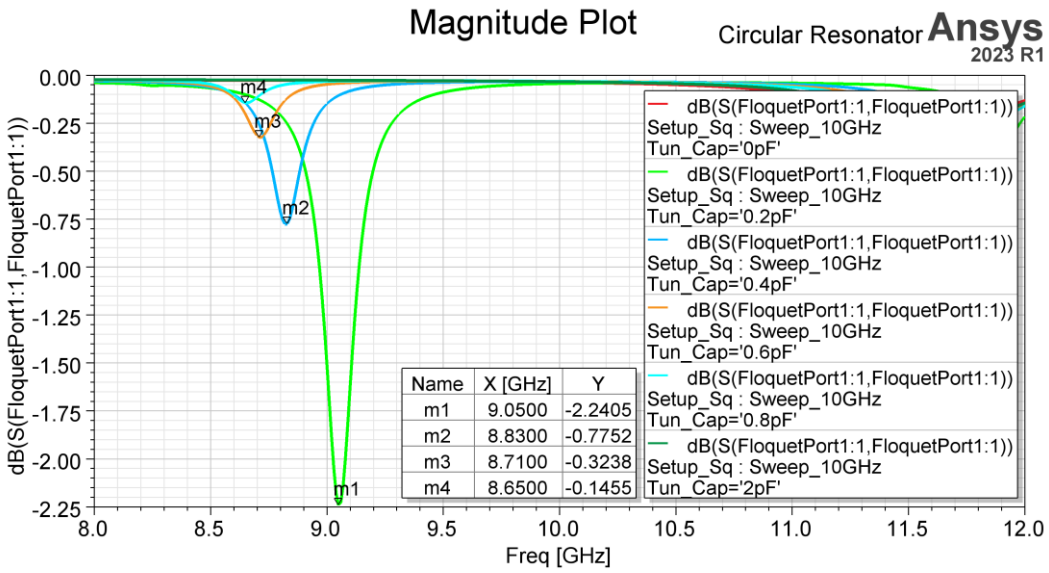

Fig 3.5 Circular Split Ring Resonator Magnitude Plot (S_{11})

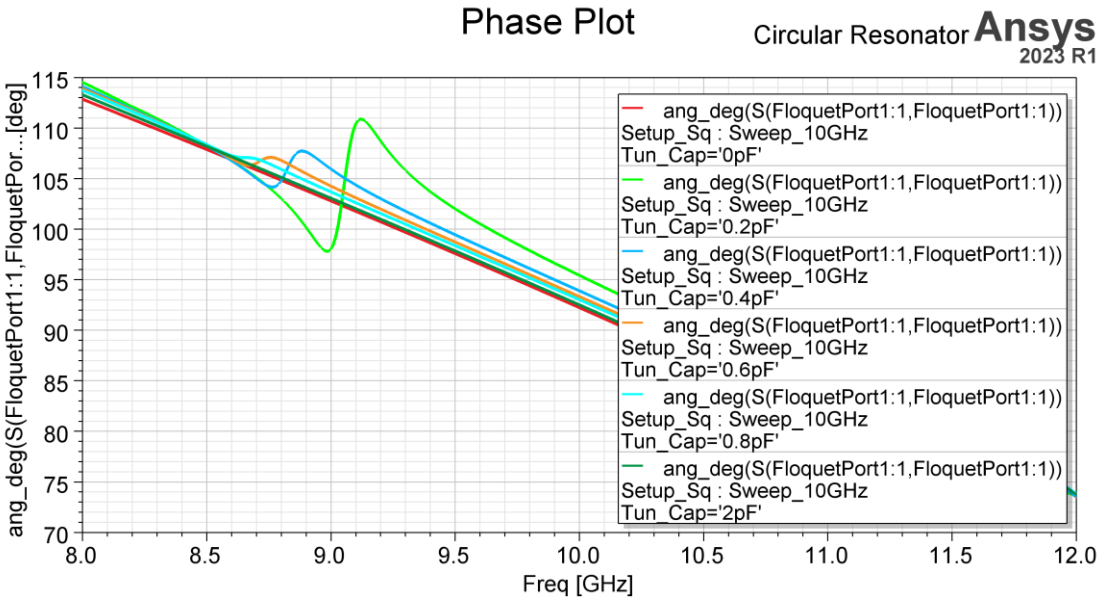

Fig 3.6 Circular Split Ring Resonator Phase Plot (S_{11})

3.5.2. SQUARE SPLIT RESONATOR

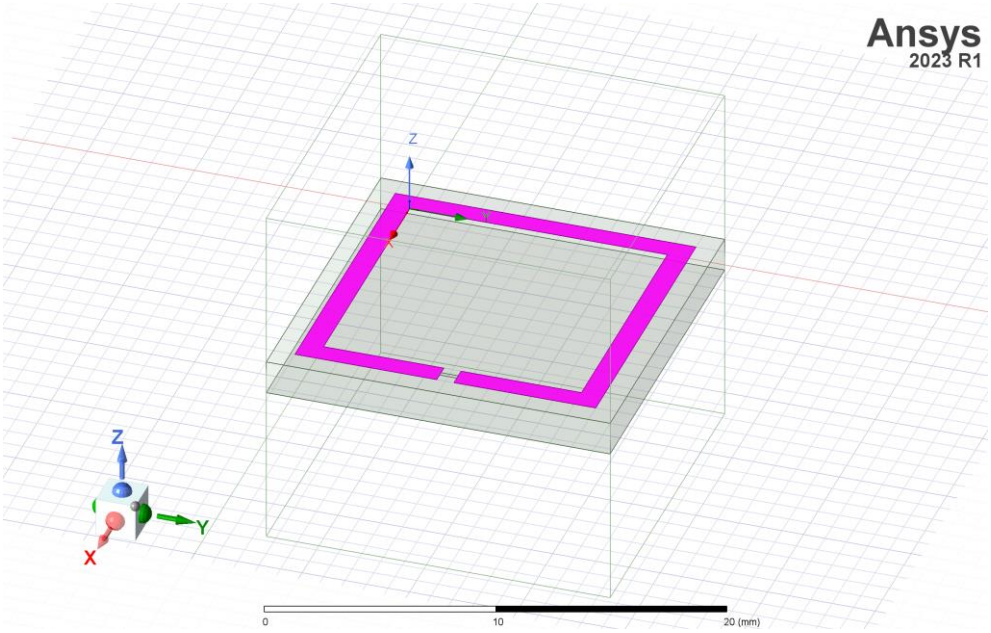

Fig 3.7 Square Split Resonator

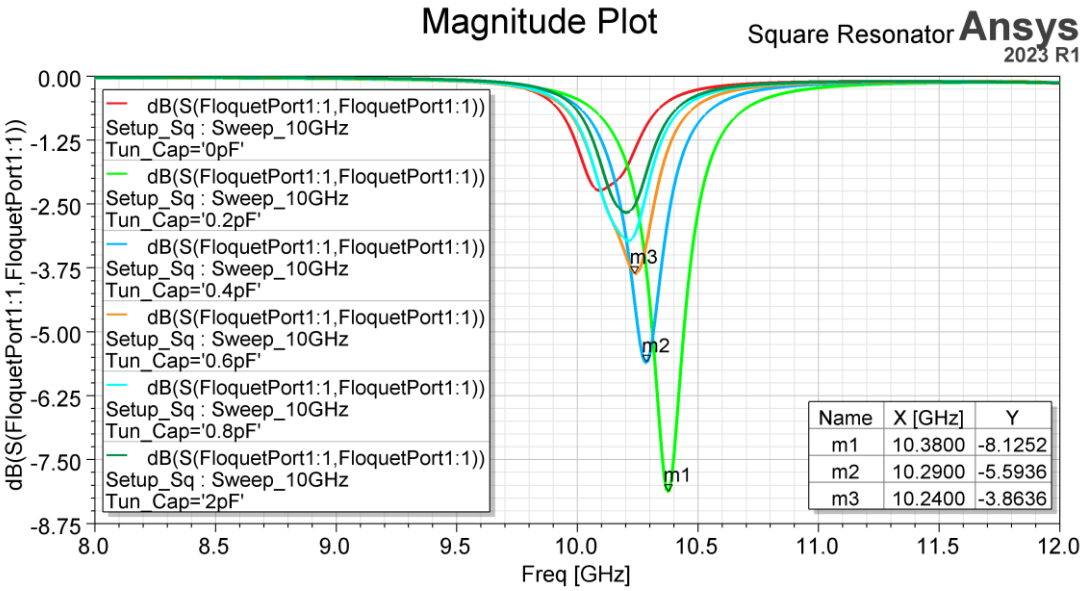

Fig 3.8 Square Split Resonator Magnitude Plot (S_{11})

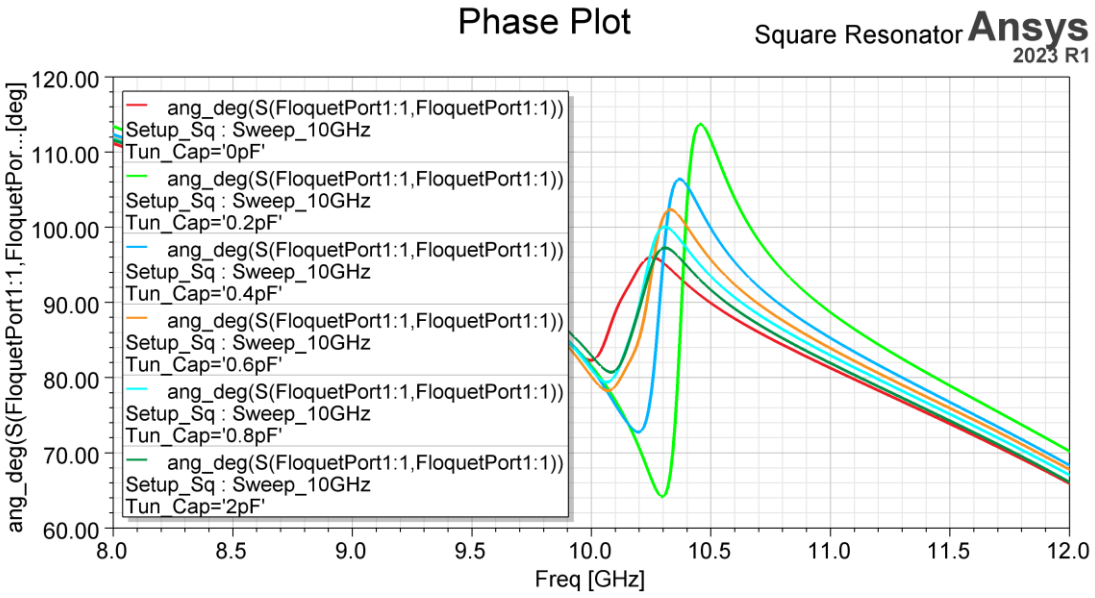

Fig 3.9 Square Split Resonator Phase Plot (S_{11})

3.5.3. TRIANGLE SPLIT RESONATOR

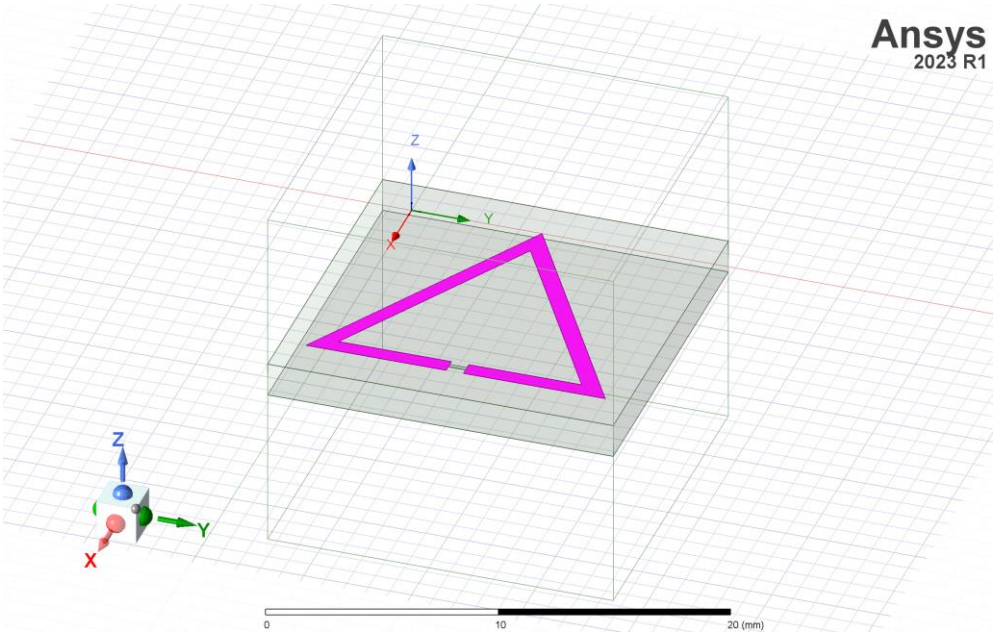

Fig 3.10 Triangle Split Resonator

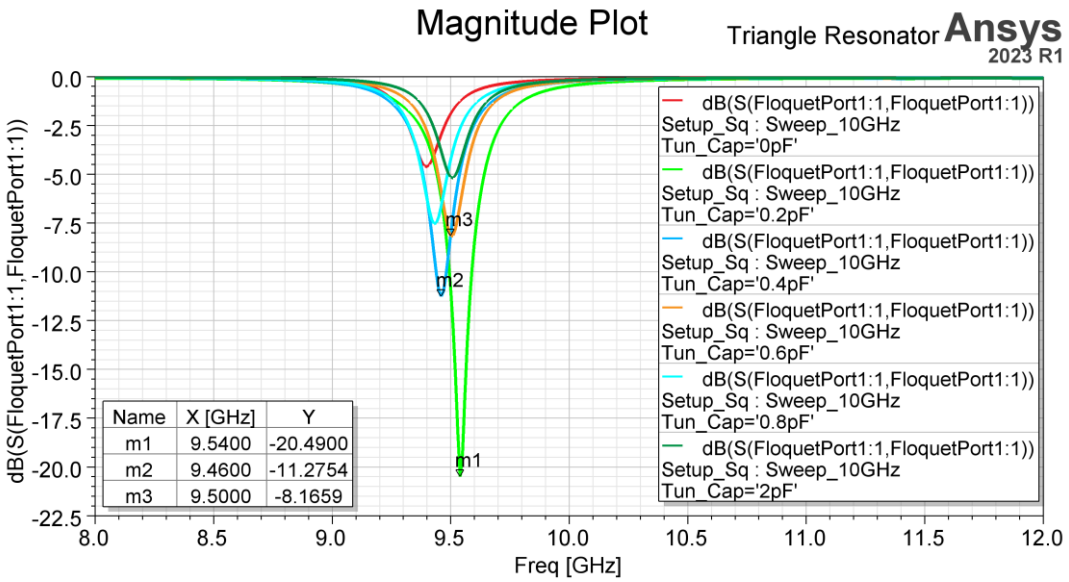

Fig 3.11 Triangle Split Resonator Magnitude Plot (S_{11})

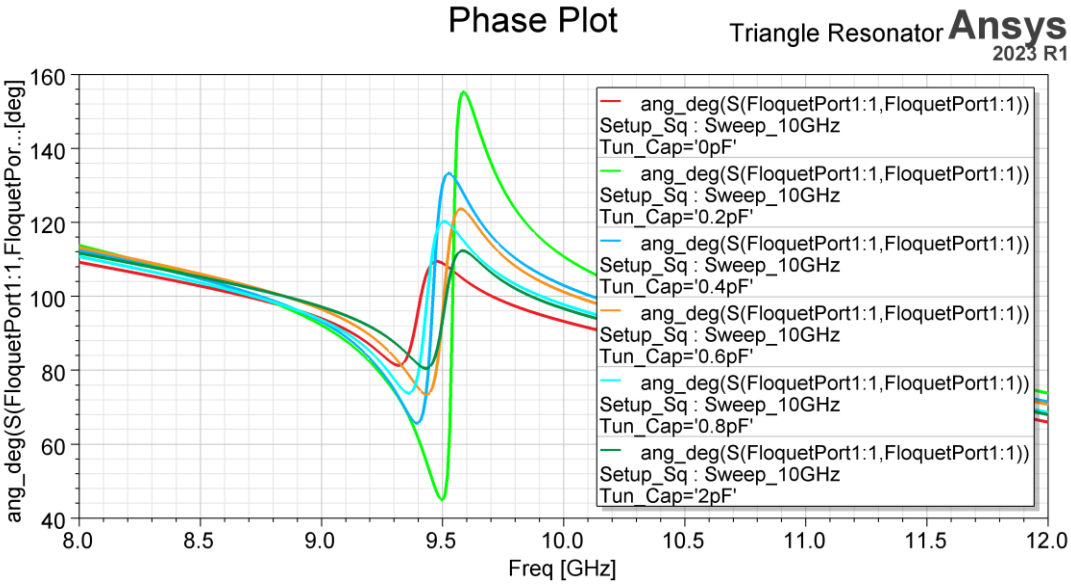

Fig 3.12 Triangle Split Resonator Phase Plot (S_{11})

3.5.4. HEXAGON SPLIT RESONATOR

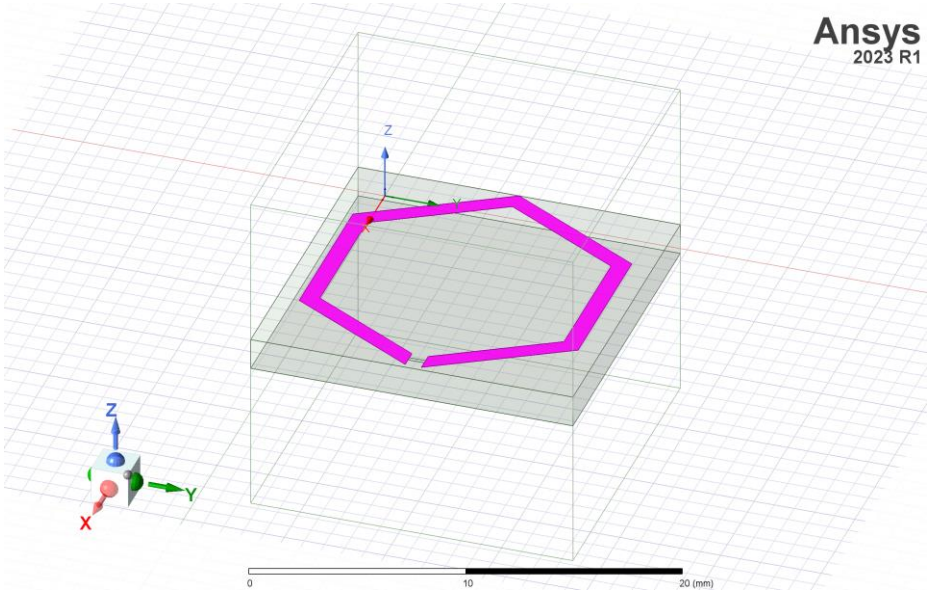

Fig 3.13 Hexagon Split Resonator

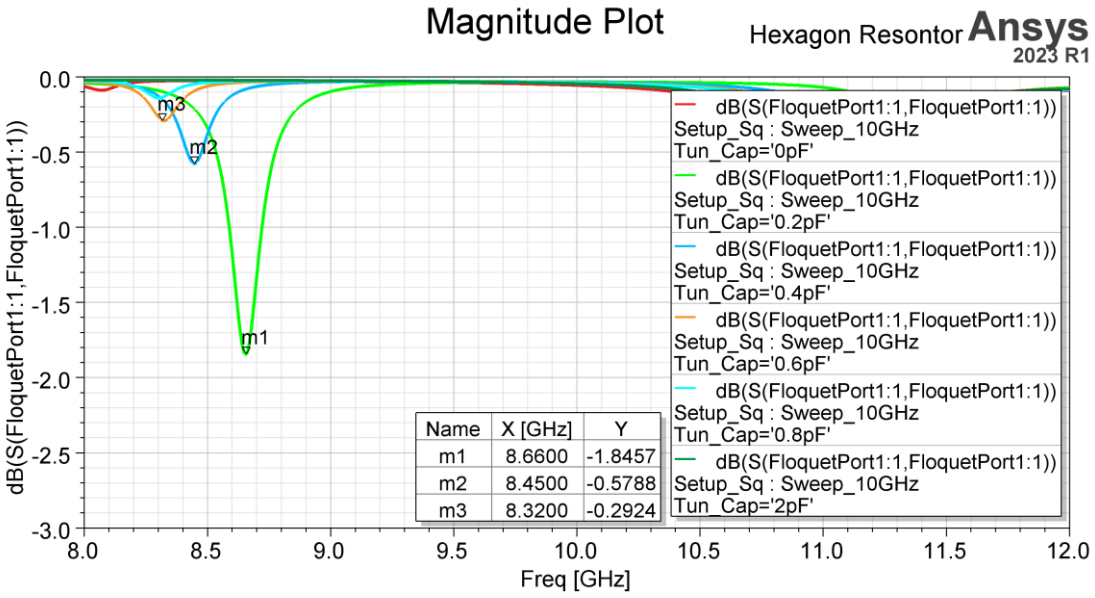

Fig 3.14 Hexagon Split Resonator Magnitude Plot (S_{11})

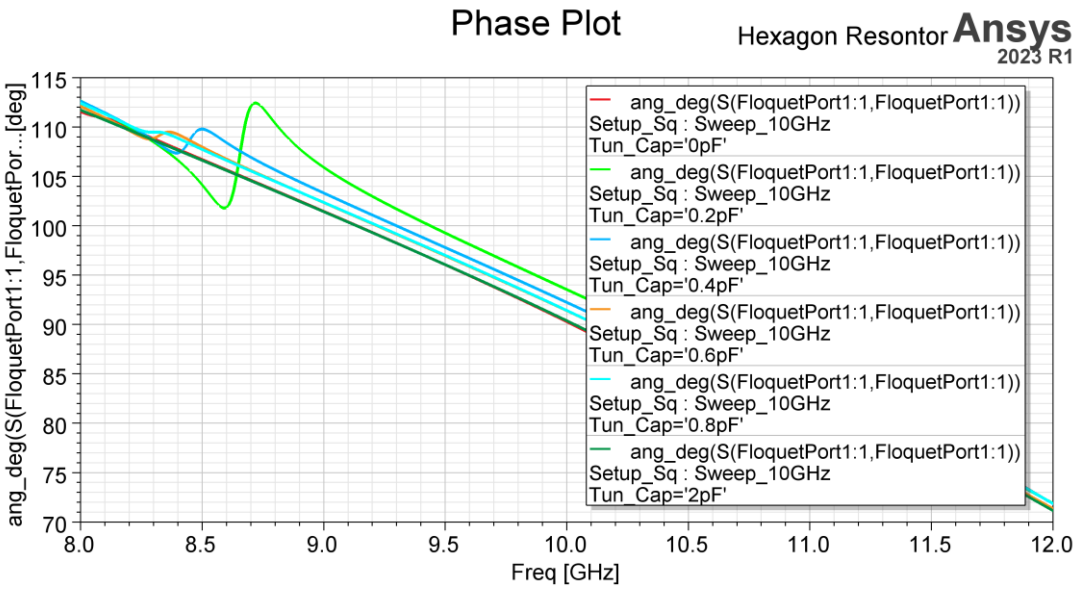

Fig 3.15 Hexagon Split Resonator Phase Plot (S_{11})

3.5.5. OCTAGON SPLIT RESONATOR

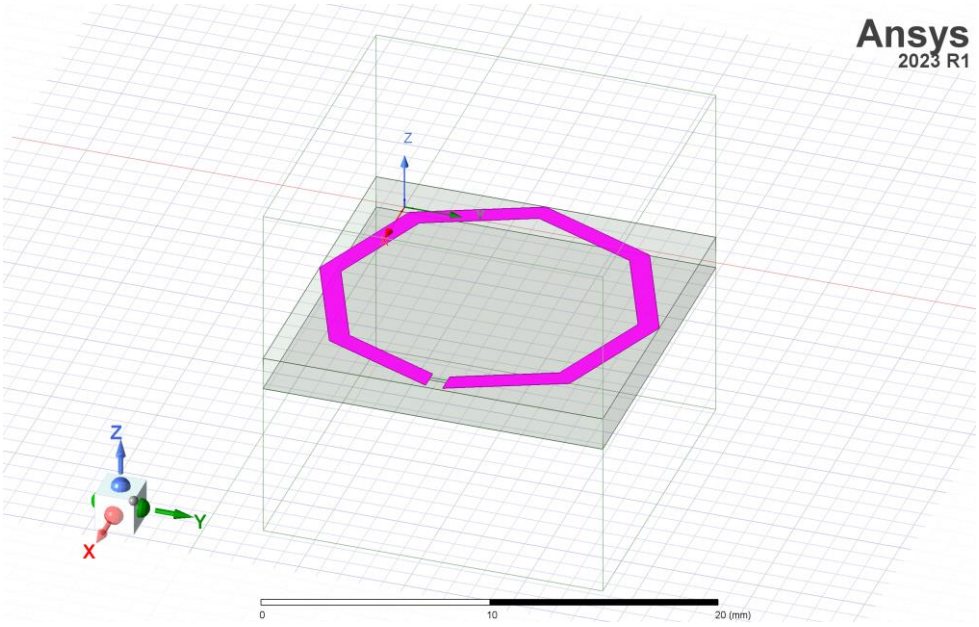

Fig 3.16 Octagon Split Resonator

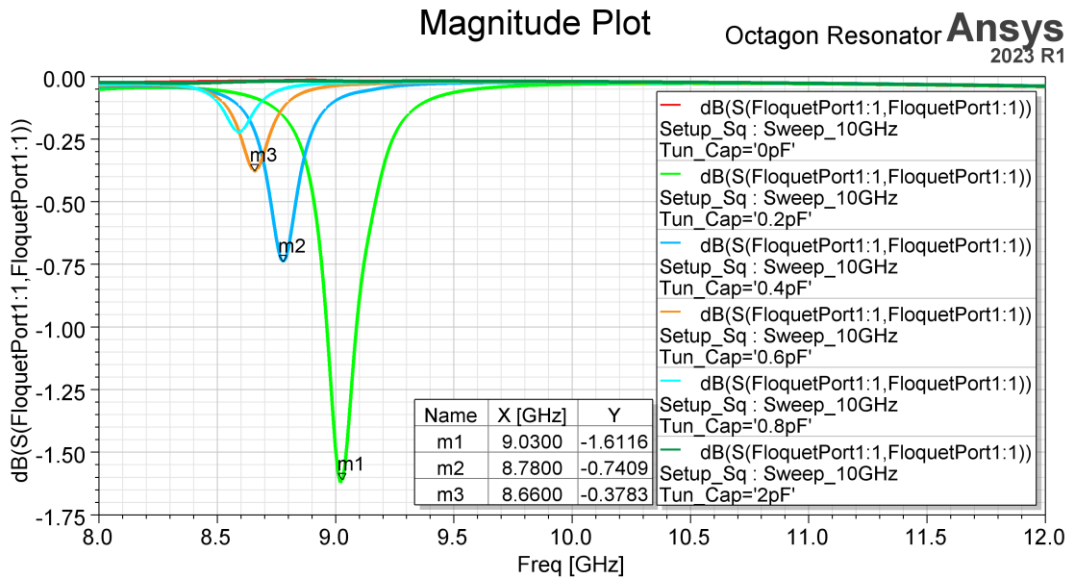

Fig 3.17 Octagon Split Resonator Magnitude Plot (S_{11})

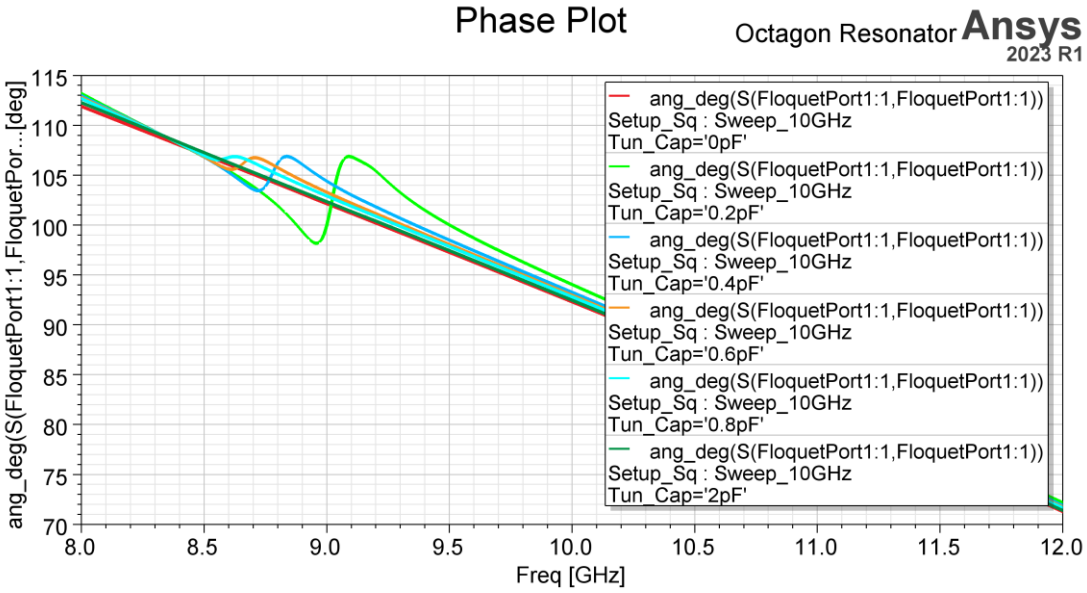

Fig 3.18 Octagon Split Resonator Phase Plot (S_{11})

3.5.6. OPTIMAL STRUCTURE FOR PRIS DESIGN

Comparing the various design structures starting from the basic circular and square split resonators to the triangle, pentagon, hexagon, octagon, omega and decagon. The optimal structure for the design of the PRIS is seen to be the octagon structure and the improved tunability in the octagon structure compared to the other polygon structure can be attributed to the following reasons

1. Symmetric structure.
2. Reduced coupling effects between the gaps.
3. Surface current generation due to edges present in the octagon ring.

A detailed comparison between various structures considered and their tunability ranges is provided in the Table 3.6.

Table 3.6 Comparison between Various SR Patch Shapes

Structure	**Power (dB)**	**Change in Frequency for Capacitance 0.2 pF to 0.4 pF**	**Change in Frequency for Capacitance 0.4 pF to 0.6 pF**
Circular Split Ring Resonator	-2.25	0.60	0.12
Square Split Resonator	-7.5	0.09	0.05
Triangle Split Resonator	-20.2	0.08	-0.04
Hexagon Split Resonator	-1.8	0.21	0.13
Octagon Split Resonator	-1.6	0.25	0.12

The next chapter 4 is attributed to design of the Passive RIS surface using the optimal structure the octagon split resonator.

CHAPTER 4

PASSIVE RECONFIGURABLE INTELLIGENT SURFACE (PRIS) - DESIGN & RESULTS

4.1. PASSIVE RECONFIGURABLE INTELLIGENT SURFACE - DESIGN

In the previous section it can be concluded that the octagon structure provides better tunability compared to other structures. The second-best candidate for the PRIS design is the square ring resonator.

4.1.1. VARACTOR DIODE PLACEMENT

Considering the practicality of fabrication, the current length cannot be used to incorporate varactor diode. Form Filipo Costa et al. by connecting the varactor diode between two adjacent diodes proved to be an efficient solution and also, provides better tunability by altering the surface currents [1, 10]. A minimum distance of 4 mm to 5 mm is considered between adjacent octogen unit cell to avoid mutual coupling.

4.1.2. IMPROVED EFFECTIVE CAPACITANCE

The placement of the diodes between the gaps of two adjacent octagonal patches give improved effective capacitance because the change in the capacitance alters the effective medium of the index which in turn alters the surface current [1, 10].

Note that the tunability can be achieved better by controlling individual capacitances but due to the simulation constraints and the availability of the processing capabilities of the system, the current simulation-based verification is limited to the tuning all the capacitance such that they all have the same capacitances.

In the next section, the designed passive 4x4 RIS surface is tuned and simulated for two values and the measurement is done at two different angles 22.5 degrees and 45 degrees to intuitively prove the change in the angle of reflection for the reflected wave.

CHAPTER 5

CONCLUSION

5.1. CONCLUSION & FUTURE SCOPE

Though the project only proves a single and most important block of the whole RIS implementation, it is necessary to note that the realization of an RIS at the Sub-6 GHz range requires both system-level implementation and channel-level consideration. Usually, the system consists of an FPGA-based controller, DAC, sensing system, and computation system. Based on the user availability inputs from the sensing system, the computational systems decide the voltage values of the individual varactor diode switches and input the necessary control signals to the FPGA, based on which the switches are tuned so that the intended angle of reflection is achieved. This ensures that the incident beam can reach the location of the UE.

The implementation of the complete RIS-based system can be pursued as future scope, not only by implementing the surface but also by improving the number of bits, considering materials that offer better tuning flexibility, and reducing mutual coupling. As described in the introduction section, the passive surface has a great advantage in terms of power consumption as it lacks the incorporation of active elements. In future research, low-power active RIS can also be a potential area, and by designing more miniaturized RIS systems, they can be used as an in-home solution, considering the rapidly increasing trend in the number of Internet of Things (IoT) devices per household.

REFERENCES

1. F. Costa and M. Borgese, "Electromagnetic model of reflective intelligent surfaces," *IEEE Open Journal of the Communications Society*, vol. 2, p. 1577–1589, 2021.

2. T. Sharma, A. Chehri and P. Fortier, "Reconfigurable Intelligent Surfaces for 5G and beyond Wireless Communications: A Comprehensive Survey," *Energies*, vol. 14, 2021.

3. C. L. Holloway, E. F. Kuester, J. A. Gordon, J. O'Hara, J. Booth and D. R. Smith, "An Overview of the Theory and Applications of Metasurfaces: The Two-Dimensional Equivalents of Metamaterials," *IEEE Antennas and Propagation Magazine,* vol. 54, pp. 10-35, 2012.

4. H. Griguer, M. Drissi, E. Marzolf, H. Lalj and F. Riouch, "Design and characterization of tunable DNG metamaterial superstrate for small beam steering antennas," *Applied Physics A,* vol. 103, pp. 895-898, June 2011.

5. C. Xu, Z. Ren, J. Wei and C. Lee, "Reconfigurable terahertz metamaterials: From fundamental principles to advanced 6G applications," *iScience,* vol. 25, p. 103799, 2022.

6. J. D. Baena, J. Bonache, F. Martin, R. M. Sillero, F. Falcone, T. Lopetegi, M. A. G. Laso, J. Garcia-Garcia, I. Gil, M. F. Portillo and M. Sorolla, "Equivalent-circuit models for split-ring resonators and complementary split-ring resonators coupled to planar transmission lines," *IEEE Transactions on Microwave Theory and Techniques,* vol. 53, pp. 1451-1461, 2005.

7. M. K. T. Al-Nuaimi and W. G. Whittow, "Compact microstrip band stop filter using SRR and CSSR: Design, simulation and results," in *Proceedings of the Fourth European Conference on Antennas and Propagation*, Barcelona, Spain, 2010.

8. A. Velez, J. Bonache and F. Martin, "Varactor-Loaded Complementary Split Ring Resonators (VLCSRR) and Their Application to Tunable Metamaterial Transmission Lines," *IEEE Microwave and Wireless Components Letters,* vol. 18, pp. 28-30, 2008.

9. A. S. Elkorany, G. T. Ahmed, D. A. Saleeb and H. A. Mohamed, "Tunable Elliptical Split Ring Resonator Using Single Varactor Diode," *Applied and Environmental Microbiology,* vol. 7, pp. 7-12, 2018.

10. L. G. da Silva, Z. Chu, P. Xiao and A. Cerqueira S, "A varactor-based 1024-element RIS design for mm-waves," *Frontiers in Communications and Networks*, vol. 4, 2023.